



# European Commission's 7<sup>th</sup> Framework Programme Grant Agreement No. **226520**

Project acronym: **COMBINE** 

# Project full title: Comprehensive Modelling of the Earth System for Better Climate Prediction and Projection

Instrument: Collaborative Project & Large-scale Integrating Project

Theme 6: *Environment* Area 6.1.1.4: *Future Climate* 

ENV.2008.1.1.4.1: New components in Earth System modelling for better climate projections

Start date of project: 1 May 2009 Duration: 48 Months

#### **Deliverable Reference Number and Title:**

D3.2: Report on the Stratosphere – Troposphere Dynamical Feedback

Lead work package for this deliverable: WP3

Organization name of lead contractor for this deliverable: Met Office

Due date of deliverable: 30 April 2012

**Actual submission date:** 

Project co-funded by the European Commission within the Seven Framework Programme (2007-2013)						
Dissemination Level						
PU	Public	PU				
PP	Restricted to other programme participants (including the Commission Services)					
RE	Restricted to a group specified by the consortium (including the Commission Services)					
CO	Confidential, only for members of the Consortium (including the Commission Services)					

### D3.2: Report on the Stratosphere – Troposphere Dynamical Feedback

#### 1. Introduction

The incorporation of a dynamically resolved stratosphere into five coupled Earth System Models (ESMs) was described in report D3.1. This report considers the stratosphere-troposphere dynamical feedbacks in these "high top" models.

Mechanisms of the influence of the extra-tropical stratosphere, acting at intra-seasonal time scales, on the tropospheric climate, are considered. To better understand the influence of the stratosphere on tropospheric climate, results from the high top model simulations are compared to those from equivalent low top models, which do not include a well resolved stratosphere.

The Southern Hemisphere tropospheric circulation, the North Atlantic Oscillation in mean sea level pressure, blocking in the Northern Hemisphere, and the downward propagation of dynamical signals from stratosphere to troposphere, are analysed in detail.

### 2. Models and simulations

Five Earth System Models are used in work package 3 (CMCC, IPSL-CM5, MPI-ESM, HadGEM, and EC-Earth). The high top versions of these models incorporate a well resolved stratosphere. Table 1 summarizes the model characteristics. The simulations carried out by these models are as described in deliverable D3.1. Here the focus is on the historical simulations and, in particular, the period from 1960 to around 2000.

	CMCC-	CMCC-	CMCC-	CMCC-	IPSL-	MPI-ESM	HadGEM	EC-EARTH
	CMS	CM	CESM	CESM	CM5		low/high-top	low/high-top
		low-top		low-top				
model	ECHAM5	ECHAM5	ECHAM5	ECHAM5	LMDz	ECHAM6	HadGEM2-CC	IFS
components	OPA8.2+LIM	OPA8.2+LIM	OPA8.2+LIM	OPA8.2+LIM	NEMO	MPIOM		NEMO2+LIM
atmospheric	T63L95	T159L31	T31L39	T31L19	96x72x39	T63L47	N96L38/N96L60	T159L62/T159L91
resolution								
	0.1. 01	2.1 21	2.1. 21	2.1. 21	2.1	1.5.1 40	1 1 401 1	1 1 401 1
ocean	2 deg x 31 levels	2 deg x 31 levels	2 deg x 31 levels	2 deg x 31 levels	2 deg	1.5 deg x 40 levels	1 deg x 40 levels	1 deg x 42 levels
resolution	icveis	icveis	icveis	icveis		icveis		
model top	0.01 hPa	10 hPa	0.01 hPa	10 hPa	70 km	0.01 hPa	39km/84km	5 hPa/ 0.01 hPa
100-1 hPa	44 levels	-	17 levels	-	1 km	15 levels	11 levels / 24	10 levels / 29 levels
resolution							levels	
stratosphere		-	orog. and non-	-	orog. and	orog. and non-	orog. and non-	orog. GWD +
	non-orog.		orog. mom. cons. GWD		non-orog.	orog. mom. cons. GWD	orog. mom. cons. GWD	Rayleigh friction
	mom. cons. GWD		coils. GWD		mom.	coils. GWD	coils. GWD	above stratop.
	GWD				GWD			
extra			ocean	ocean		carbon cycle	ocean and land	
components			2	biogeochemistry		with	carbon cycle;	
1			and land	and land		land vegetation	aerosols	
			vegetation	vegetation		and ocean		
			carbon cycle	carbon cycle		biogeochemistry		

 Table 1: Summary of the WP3 high and low top models

#### 3. Results

# 3.1 Modelled changes in the Southern Hemisphere: Role of stratospheric dynamics

Observed large changes in the Southern Hemisphere (SH) climate over the past few decades are characterized by a shift in the Southern Annular Mode (SAM), especially during summer (December-January-February; DJF). Model studies (e.g. Son et al., 2010) have found that during the SH summer these changes can be mostly attributed to stratospheric ozone depletion. The following analysis looks at how well these changes are reproduced in the historical simulations of the high and low top CMCC models and the high top IPSL model.

Figure 1 shows temperature changes for the two CMCC high top models and the two CMCC low top models area averaged poleward of 64°S from the surface up to 20 hPa. Linear trends are shown for the period 1960-1999, as in Son et al. (2010) and Gerber et al. (2010). In agreement with previous modelling studies and observations, the two models show a cooling of the lower stratosphere, with maximum in November, one month after the peak in the imposed ozone trend. The main difference between the two sets of model simulations is that the cooling for the two high top models (~2.5-3 K/decade) is about 1.5 times larger than the cooling found in the two low top models. This difference arises because the total cooling in the high top models is due to the radiative cooling related to the imposed ozone, plus less adiabatic warming due to reduced downwelling (not shown) that is not found in the low top models. The absence of a dynamical stratosphere leads to less net cooling associated to stratospheric ozone depletion.

Through thermal-wind balance, changes in the meridional gradient of the zonal mean temperature are accompanied by changes in the vertical shear of the zonal mean zonal wind, leading to an acceleration of the polar vortex, as shown in Figure 2. The stratospheric westerlies are enhanced in November and the tropospheric jet is stronger down to the surface in Nov-Dec (high top models). The two low top models show different changes, with trends in the zonal mean zonal winds in the lower stratosphere much reduced. The response at the surface is also different, with no changes in DJF for the high-resolution low top model and a delayed response for the low-resolution one. For the latter model, the surface trends in the winds appear to be associated with the long-lasting cooling that is found in both the troposphere and the stratosphere for the entire year (see Figure 1, upper right panel).

Mean Sea Level Pressure (MSLP) decreases over Antarctica and increases at 40°S (not shown). This pattern suggests that for this period (1960—1999) the SH trends projected onto a positive SAM phase, in good agreement with the patterns and amplitude of the anomalies simulated by both the high top and low top models. Figure 3 shows the time series of the SAM index, here defined as the difference in normalized DJF MSLP between 40°S and 65°S (after Gong and Wang, 1999). The anomaly is shown for 3 high top models and 1 low top model (the IPSL high top results are an average of an ensemble of 4 members). The DJF trends are about 1.5 to 2 times larger for the high top models than for the low top one, in better agreement with the NCEP and ERA-40 trends, though for a different period (1979-1999).

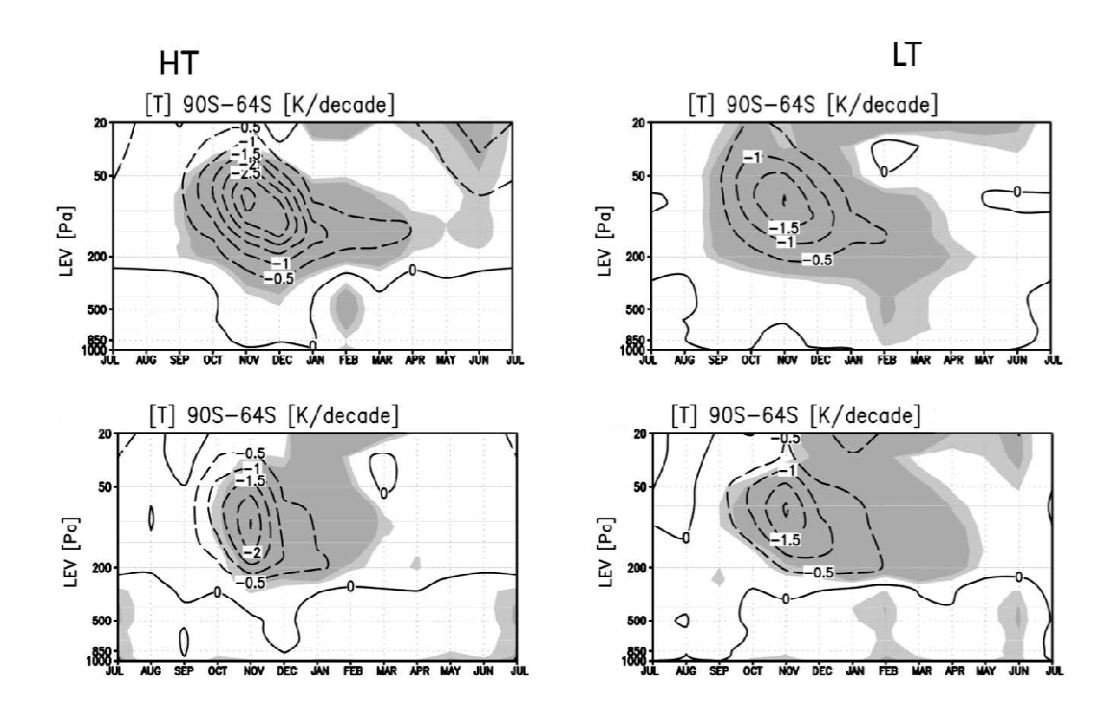


**Figure 1:** Linear trends of the monthly mean zonal mean temperature averaged poleward of 64°S for the two CMCC high top models (left) and the two CMCC low top models (right). The mean trends are computed for 1960 to 1999. Contour intervals are 0.5 K/decade. Trends that are statistically significant at the 95% level are shaded. Top panels show CMCC-CESM, and bottom panels show CMCC-CMS.

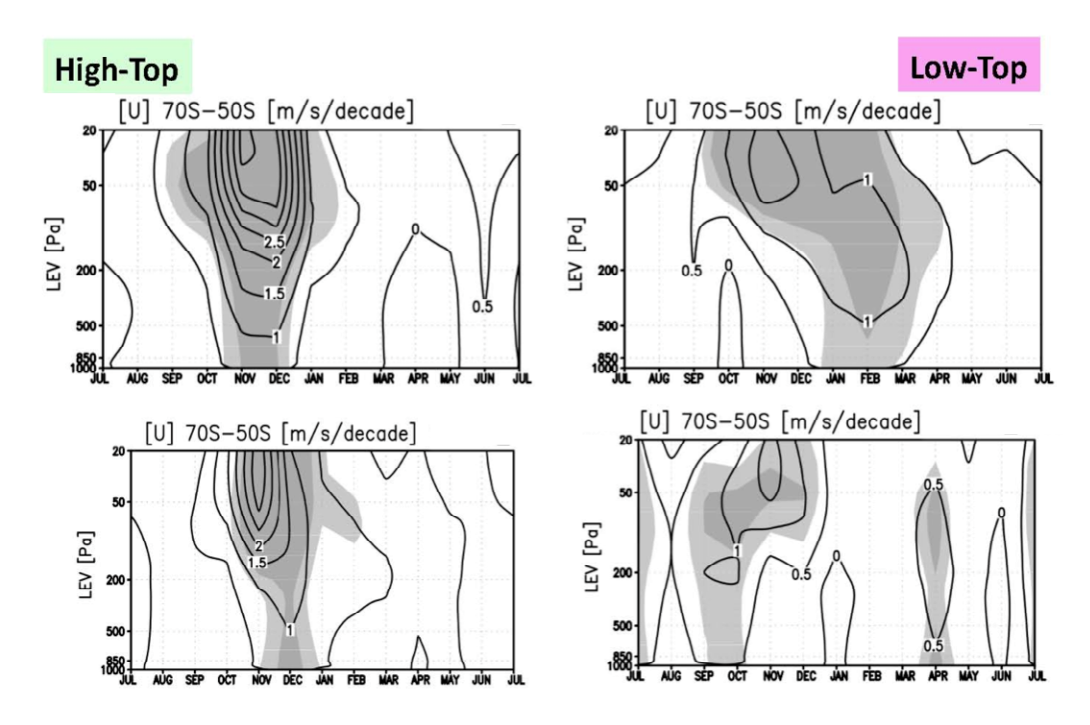


**Figure 2:** As Figure 1, but for the zonal mean zonal wind, 70-50°S.

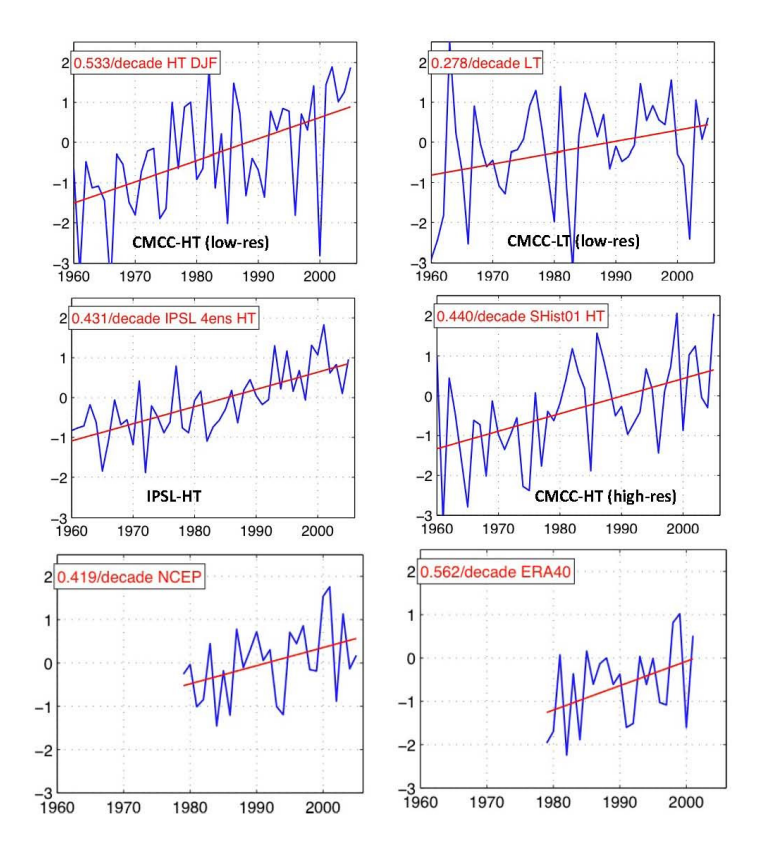


**Figure 3:** Time series of the SAM index [defined as the difference in normalized DJF sea level pressure between 40°S and 65°S after Gong and Wang (1999)]. The anomaly is calculated with respect to 1979-1999.

#### 3.2 North Atlantic Oscillation

The North Atlantic Oscillation NAO (Osborn and Jones, 2000) is known to influence temperature, precipitation and cloudiness over northern Europe due to the resultant change in the position of the North Atlantic storm track (Folland et al., 2009). As such the predictability of the NAO is of interest to seasonal forecasting, and the long-term trends in the NAO are of relevance for climate change.

An index of NAO variability is calculated from MSLP over the Azores (27°W, 37.5°N) minus MSLP over Iceland (20°W, 64°N). Figure 4 shows the detrended interannual standard deviation in this NAO index calculated for DJF, 1960–2000, for the five high top models, two low top models, and ERA-40 (Uppala et al., 2005). All models show realistic interannual variability in the NAO.

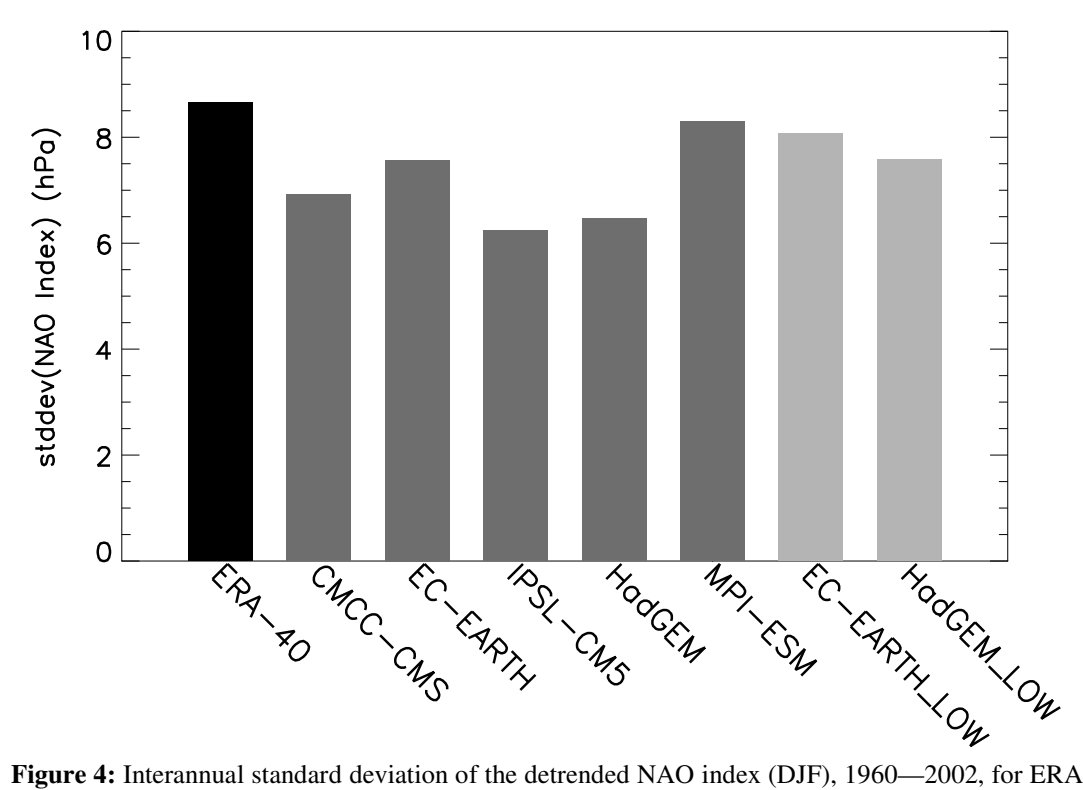


**Figure 4:** Interannual standard deviation of the detrended NAO index (DJF), 1960—2002, for ERA-40 (black), high (dark gray) and low (light gray) top ESMs.

Low frequency variability in the NAO index has been linked to changes in stratospheric zonal mean zonal wind, U, (Wallace, 2000; Scaife et al., 2005). Figure 5 shows a scatter plot of the trend in the NAO index versus the trend in U(60°N, 50hPa) for 1960–2002. All points lie approximately on a straight line through the origin suggesting a strong link between the trends in these two parameters. The average interannual correlation between the NAO index and U in the high top models is around 0.55 (Table 1), and though the correlation in CMCC-CMS is somewhat lower at 0.30, this is still significant at the 95% level. Table 1 also shows that the correlation in the EC-Earth and HadGEM low top models, at 0.42 and 0.24 (0.24 is not statistically significant at the 95% level), is somewhat lower than that in the equivalent high top models, 0.53 and 0.60 respectively, demonstrating that a raised upper boundary can significantly improve the link between the NAO index and stratospheric jet strength.

Figure 6 shows MSLP regressed onto a normalised NAO index for ERA-40 and high and low top versions of HadGEM and EC-Earth. The mean of three ensemble members is shown for HadGEM. The observed dipole structure in the north Atlantic is more accurately simulated by the high top models, with centres of action around 20°W as observed, as opposed to around 30°W in the low top models. There is also a region of high MSLP over the north Pacific in positive NAO years in the high top models. This increased midlatitude Pacific signal (150°W—180°W) in a model with a better resolved stratosphere is consistent with the work of Dong et al. (2010) which shows enhanced MSLP anomalies in the Pacific during times when the NAO signal penetrates more deeply into the stratosphere. Furthermore, the high top model shows a more realistic response over Asia with anomalously negative MSLP in positive

NAO years. Thus the teleconnections responsible for capturing an accurate spatial response to the NAO are better captured with a high top model.

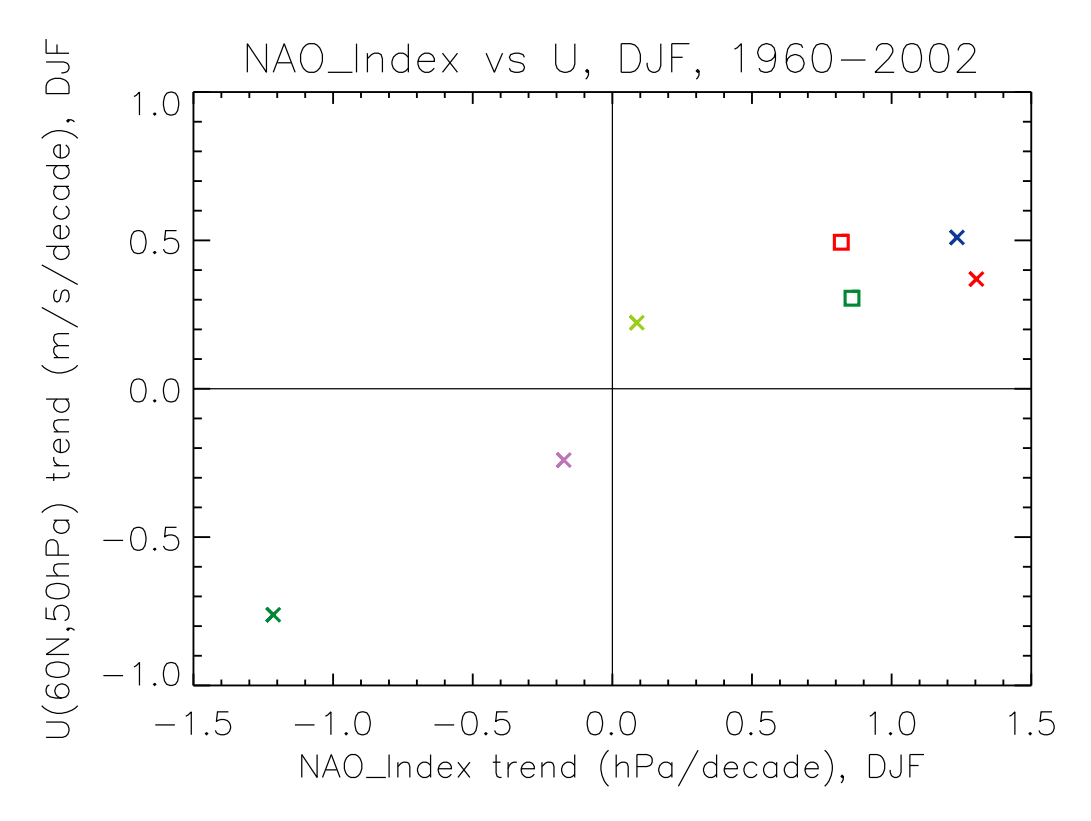


**Figure 5:** Scatter plot of the trend in the DJF NAO index versus the trend in zonal mean zonal wind, U(60°N, 50hPa), for 1960–2002. High top models shown as crosses. Low top models shown as squares.

	High top model							
	CMCC-CMS	EC-EARTH	IPSL-CM5A-LR	METO	MPI-ESM-LR			
Total corr	0.30	0.53	0.53	0.60	0.63			
Interannual corr	0.30	0.52	0.53	0.58	0.63			
	Low top model							
		EC-EARTH		METO				
Total corr		0.43		0.25				
Interannual corr		0.42		0.24				

**Table 2:** Correlations between the NAO index and U(60°N, 50hPa), 1960—2002. Total correlations (raw timeseries) and interannual correlations (detrended timeseries) are shown.

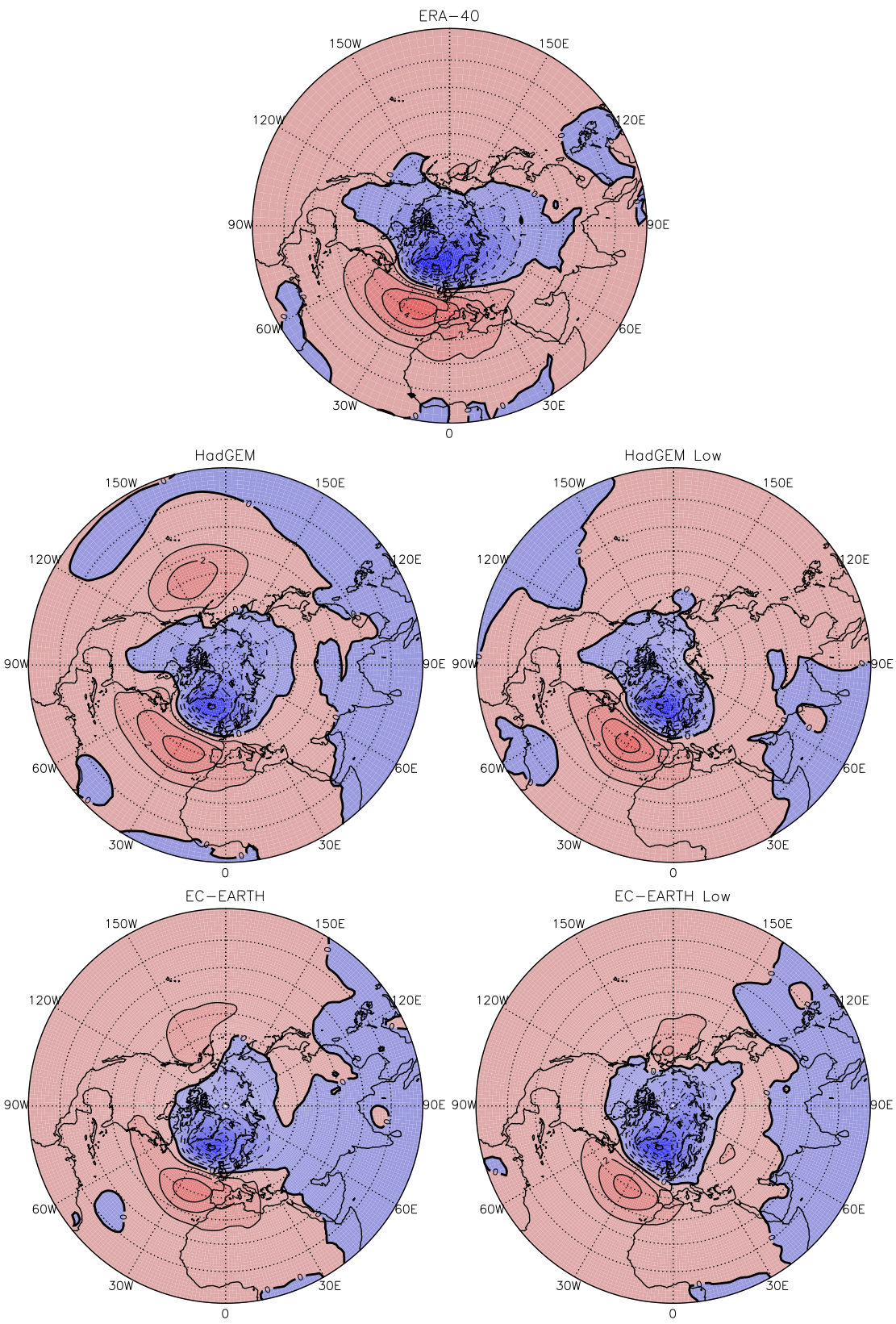


Figure 6: Mean Sea Level Pressure regressed onto a normalised NAO index for ERA-40 and high and low top versions of HadGEM (ensemble mean) and EC-Earth.

# 3.3 Northern Hemisphere Blocking

Blocking of the tropospheric jet stream is often associated with persistent spells of anomalous weather (Buehler et al., 2010; Sillmann et al., 2011), and changes in the behaviour of tropospheric blocking activity under climate change may contribute to future changes in regional weather and climate (Woollings et al., 2010). A persistent problem with coupled general circulation models (GCMs) is the existence of substantial biases in their representations of blocking (D'Andrea et al., 1998; Scaife et al., 2010). These biases naturally call into question these models' ability to provide accurate estimates of blocking activity in the future climate.

Like previous generations of models, the work package 3 models (Table 1) exhibit large blocking biases. Much of this bias is related to errors in the climatological mean state of the models. Such mean-state error may or may not be related to the models' representation of synoptic eddies themselves. One possible factor affecting blocking is the representation of the stratosphere in the models. To investigate this possibility, high-top (HT) and low-top (LT) versions of the models are compared.

Model biases are computed by comparing climatologies of the models' historical experiments against the climatology of the ECMWF ERA-40 reanlaysis data (Uppala et al., 2005), where the climatologies are computed for the years covering the whole ERA-40 period, comprising Northern Hemisphere (NH) winters from 1957-2001 (where the year number denotes the year in which the winter begins). Unless stated otherwise, all analysis utilizes the December-January-February (DJF) period.

Blocking is diagnosed using a blocking index derived from daily 500 hPa geopotential height, Z500, according the method of Tibaldi and Molteni (1990) as generalized to vary in both latitude and longitude by Scherrer et al. (2006). At each latitude φ and longitude  $\lambda$ , the equatorward meridional gradient of Z500 is estimated as GHGS =  $[Z500(\lambda, \phi) - Z500(\lambda, \phi - \Delta\phi)] / \Delta\phi$ , where  $\Delta\phi = 15^{\circ}$  as in Scherrer et al. (2006). The poleward gradient is similarly defined as GHGN =  $[Z500(\lambda, \phi + \Delta\phi) - Z500(\lambda, \phi)]$  / Δφ. Using Z500 from 10°N to 90°N, GHGS and GHGN are determined at latitudes from 25°N to 75°N. An "instantaneous blocking" (IB) event is defined to occur when two conditions are fulfilled: (1) GHGS > 0, indicating reversal of the climatological gradient of Z500 with easterlies equatorward of  $\phi$ , and (2) GHGN < -10m/° latitude, indicating strong westerlies poleward of  $\phi$ . The IB index is defined to be 1 when these two conditions are satisfied, and 0 otherwise. Additional filters may then be applied to this index in order to select events of desired spatial extent and duration. Following Scherrer et al. (2006), only a 5-day minimum duration filter is applied. The time mean of the index is the blocking frequency in events per day, which can be expressed as a percentage of blocked days.

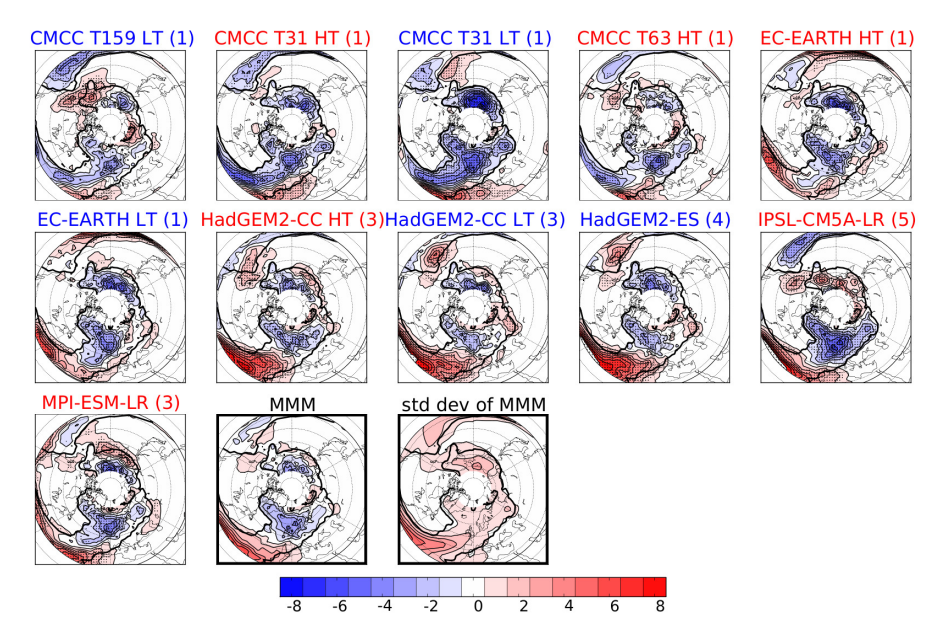


**Figure 7:** Model climatological blocking biases: model climatology (red titles denote high top models and blue titles denote low top models) minus ERA-40 climatology, for DJF in the 1957-2001 period. Positive (negative) differences are shown in red (blue) with contour interval 1% (percentage of blocked days). Model climatologies are computed as ensemble means when more than one ensemble member for a given model is available; the number of ensemble members for each model is indicated in brackets following the model name. For the individual models, stippling denotes 95% statistical significance using a two-sided t-test. The 1% contour of the ERA-40 climatology is superimposed on all plots. The last two panels show the multi-model mean (stippling of significance levels is omitted) and the inter-model standard deviation. Models as in Table 1, except HadGEM2-ES for which data from the CMIP5 archive is used.

Biases of DJF climatological blocking in the historical simulations during the ERA-40 time period (1957-2001) are shown in Figure 7. All models underestimate the frequency of European blocking, consistent with previous multi-model blocking assessments (D'Andrea et al., 1998; Scaife et al., 2010). Biases at lower latitudes in the Atlantic are generally positive (e.g., HadGEM2-CC), and in some cases form a negative-positive west-east dipole (e.g., CMCC models) that tilts eastward with increasing latitude. A dipolar bias suggests a geographical shift in blocking activity and a tilted dipole suggests a relation between the bias and the tilt of the Atlantic jet, which is often poorly represented in models (Woollings and Blackburn, 2012). Biases in the Pacific basin vary more widely amongst the models. In general, biases are of comparable magnitude to the observed climatology, for example negative European blocking biases of more than 50% of the observed magnitude are common. Most of the blocking biases lie within regions in which blocking is observed, although most models also have some amount of blocking occurring outside these regions.

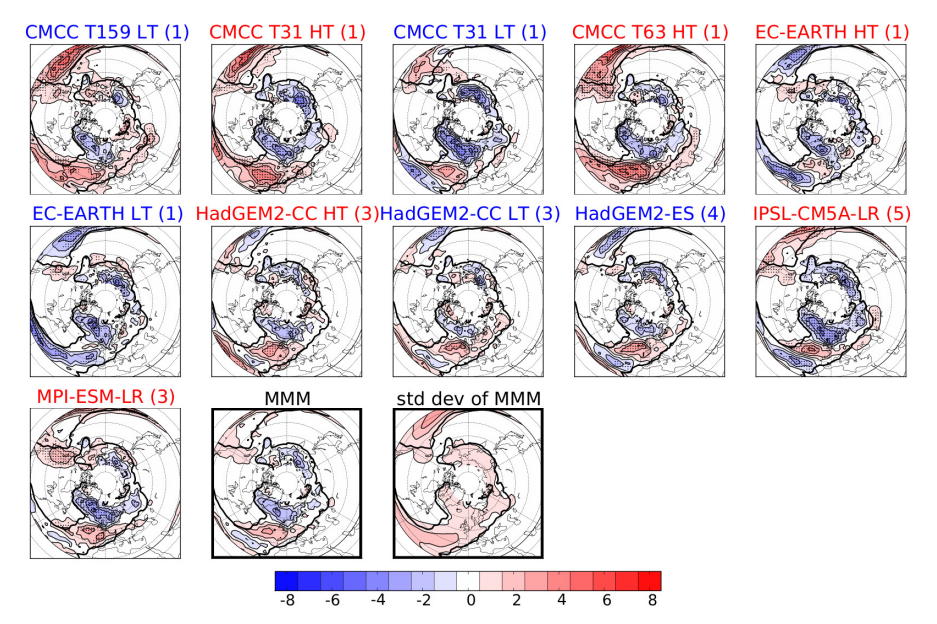


**Figure 8:** As Figure 7, but for model biases re-calculated after applying the bias correction methodology of Scaife et al. (2010) to the models' blocking frequencies.

The last two panels of Figure 7 show the bias of the multi-model ensemble mean, as well as the inter-model standard deviation (i.e., the standard deviation of the distribution of model means, or equivalently, of model biases). The multi-model mean summarizes the features noted above: a deficit of European blocking, a surfeit of low-latitude Atlantic blocking, and no clear signal in the Pacific except perhaps a common tendency for the models to overestimate the frequency of blocking over the west coast of North America. Large (small) values of the inter-model standard deviation indicate regions where the models generally disagree (agree) with each other: the North Pacific, low-latitude Pacific, and to some extent high-latitude Atlantic blocking are all regions where the bias varies between models. The large inter-model standard deviation in the low-latitude Atlantic also indicates some divergence amongst the models, but note that the mean bias values here are also large.

Scaife et al. (2010) argued that when blocking events are defined relative to an absolute threshold, such as a change in sign of the meridional gradient of geopotential height (GHGS), model biases in blocking frequency may indicate biases in both the mean state and the variability. Since blocking frequency is intended to measure variability, it is desirable to diagnostically separate the contributions of the mean state and the variability to the overall bias. Scaife et al. (2010) separated mean state bias and variability bias by re-calculating the blocking indices of models after shifting their probability density functions to remove mean-state biases (i.e., by subtracting each model's climatological mean state and adding the resulting anomalies to the observed climatological mean state). The blocking index thus defined is a measure of the variability of the models.

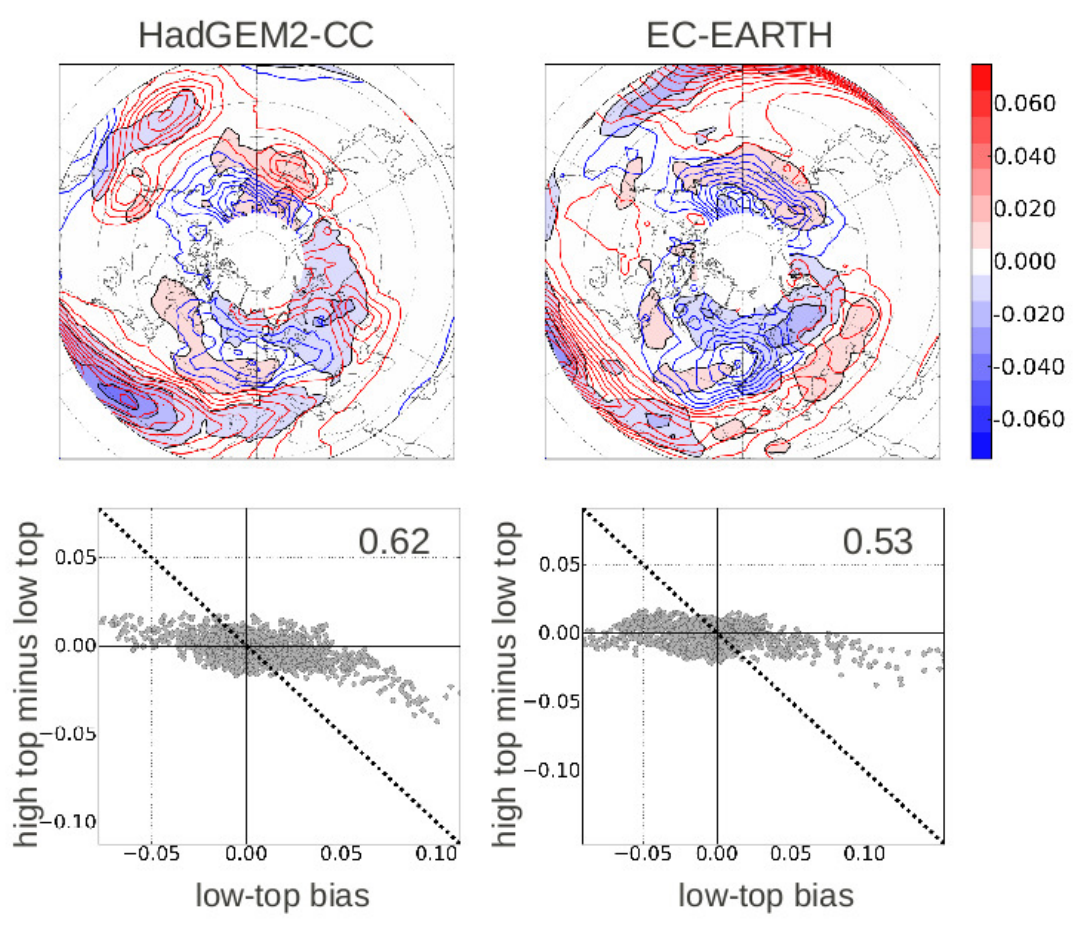


**Figure 9:** High-top minus low-top IB differences (HT-LT), shown in filled contours, and LT bias (defined as the model minus ERA-40), shown in line contours. Contour interval (0.01 events/day) is the same for both HT-LT and LT bias. Below each contour plot is shown the scatter, over all horizontal gridpoints, of the HT-LT vs. LT bias. The number in the upper right corner of each scatter plot gives the fraction of gridpoints that fall into the oppositely-signed quandrants (i.e. upper left and lower right quandrants): points lying in these regions indicate that the HT model has a reduced bias compared to the LT model.

Figure 8 shows the result of applying this bias-correction. Regions where the biascorrected blocking frequencies differ from observed blocking – i.e., where the biascorrected blocking frequency retains a non-zero bias - are regions in which the distribution of the models' variability differs from that of ERA-40. Figure 8 shows an overall reduction in blocking bias compared to Figure 7. This suggests that a large amount of model bias is associated with biases in the mean state of Z500 [as found with earlier models by Scaife et al. (2010)]. However, a significant amount of bias still remains, much of which is unlikely to be due to sampling variability. Indeed, many locations show biases that are of similar magnitude to the original biases (even though an overall reduction across the hemisphere is nevertheless apparent). This may indicate the influence of the background time-mean state on eddy life cycles involving wave breaking, which are expected to respond to ambient mean-flow conditions (Thorncroft et al., 1993). The fact that biases remain after applying bias correction to the models' mean states indicates that the models differ from observations in terms of both mean and variability, even if the mean state is the dominant source of bias in many regions.

The high and low top versions of HadGEM2-CC and EC-EARTH differ only in model lid height and vertical resolution. This allows a controlled high versus low top comparison. Figure 9 shows the HT-LT differences in the instantaneous blocking (IB) frequency for these two models. It is striking that two separate models, which do not share a common history of model development, exhibit very similar HT-LT differences. Furthermore, performing the same analysis with another coupled GCM for which a controlled comparison of HT and LT experiments is available (120-year integrations of HT and LT versions of the Canadian Middle Atmosphere Model; not shown) also reveals a similar HT-LT difference. This increases confidence that the HT-LT difference represents a robust physical effect, though further work is required to identify the mechanism through which improved representation of the stratosphere leads to this change in blocking frequency. Comparing the HT (T63) and LT (T159) versions of the CMCC model also reveals a similar difference in the North Atlantic sector (not shown). The fact that these uncontrolled comparisons yield a similar signal as the controlled comparisons shown in Figure 9 suggests that the effects of the stratosphere are robust against other model changes.

It is desirable to assess the change in model bias associated with improved stratospheric representation in the HT models. Biases of the LT model versions are shown as superimposed line contours in Figure 9. Regions in which the HT-LT bias is of opposite (same) sign to the LT bias indicate where the HT model version has reduced (increased) bias compared to the LT. Comparison of the overall magnitude of the HT-LT difference and the LT bias indicates that the HT-LT difference is in most locations not large compared to the overall bias. Furthermore it is apparent that the HT bias is reduced in some regions compared to the LT bias, but increased in others. The scatter plots in the bottom row of Figure 9 quantify the overall change in bias between the HT and LT model versions by showing the scatter, across all horizontal gridpoints, of the HT-LT difference vs. the LT bias. The overall negative slope of the scatter indicates an overall reduced bias in the HT models, although the improvement is marginal in EC-EARTH. However, the weak slope of the relationship indicates, as already seen from the contour plots, that HT-LT differences are generally weak compared to the overall bias.

# 3.4 The northern hemisphere polar vortex

### 3.4.1 Downward propagation

In winter mid-latitudes zonal mean wind anomalies propagate downward from the upper stratosphere to the surface on a time-scale of a week to a few months (Baldwin and Dunkerton, 1999; Christiansen, 2001). Although the mechanism of the downward propagation is still disputed – in particular the propagation from the lower stratosphere to the surface – and several mechanisms have been suggested (e.g., Christiansen, 1999; Ambaum and Hoskins, 2002; Perlwitz and Harnik, 2004; Song and Robinson, 2004) its potential for extended range forecasts has drawn substantial interest (Baldwin et al., 2003; Charlton et al., 2003; Christiansen, 2005; Siegmund, 2005).

While at least some climate models include a good representation of the downward propagation it is not obvious what the requirements for a good representation are. This is related to the fact that both the tropospheric wave forcing and the stratospheric

conditions are important for the downward propagation. This was, for example, shown in Christiansen (1999), in perpetual January experiments with a general circulation model. It has also been demonstrated (Christiansen, 2005) that simple statistical forecasts based on stratospheric information perform as well as a state-of-the-art dynamical seasonal forecast model when forecasting the surface zonal mean zonal wind at 60°N and the temperature in northern Europe. The stratosphere-troposphere coupling might therefore offer an important contribution for improving dynamical forecasts when it is properly implemented in the forecast system.

The differences in the downward propagation in the historical experiments from high and low top versions of EC-Earth (Hazeleger et al., 2011) and HadGEM, and the two high top versions of CMCC, are investigated. For EC-Earth and HadGEM the only differences between the high and low top versions are in the vertical resolution and in the top of the model atmosphere. For CMCC the two model versions differ in horizontal and vertical resolution but have the same model lid height.

The average properties of the downward propagation can be summarized by calculating the lagged correlations between the zonal mean zonal wind at 60°N and 10 hPa and the zonal mean zonal wind at all other levels at 60°N [calculations are, if not otherwise stated, based on daily means for the Northern Hemisphere winter (December, January, February) season]. These lagged correlations are shown in Figure 10 for all experiments based on the period 1900-2005; low top experiments in the left column (EC-Earth and HadGEM) and high top experiments in the right column. The lagged correlations are also shown for the ERA-40 reanalysis for the period 1960-2005. As in Christiansen (2005) the statistical significance of the correlations is calculated with a Monte-Carlo method comparing the original timeseries with a batch of 500 artificial time-series with the same auto-correlation spectrum as the original time-series.

Note the remarkable similarity between all models (both high top and low top) and the reanalysis. The downward propagation, evidenced by the tilt of the correlations, is clearly seen in all panels of Figure 10. Statistically significant signals are seen near the surface in all models and these correlations have values of around 0.1–0.2. Weak correlations in the middle of the troposphere are seen in all models. These features are observed in other observational studies although they are less clear in the ERA-40 data in Figure 10.

Comparing the low top and high top versions of each model reveals several differences. For the EC-Earth model only small differences are found between the two versions and both versions compare well with the ERA-40 reanalysis. This is not surprising as even the low top version of EC-Earth has a well resolved stratosphere, at least up to 5 hPa. For the low top version of the HadGEM model the time-scales in the stratosphere are too long when compared to the ERA-40 reanalysis. This has improved in the high top version which is now very similar to both the EC-Earth model and the reanalysis. The CMCC model shows the largest differences between the two model versions. For this model the time-scales in the stratosphere differ drastically between the two versions. They are too long (compared to the ERA-40 reanalysis) in the low resolution version and too short in the high resolution version (EC-Earth and HadGEM differ in vertical resolution; it should be remembered that the

two model versions of CMCC differ in the vertical and horizontal resolution but not in model lid height).

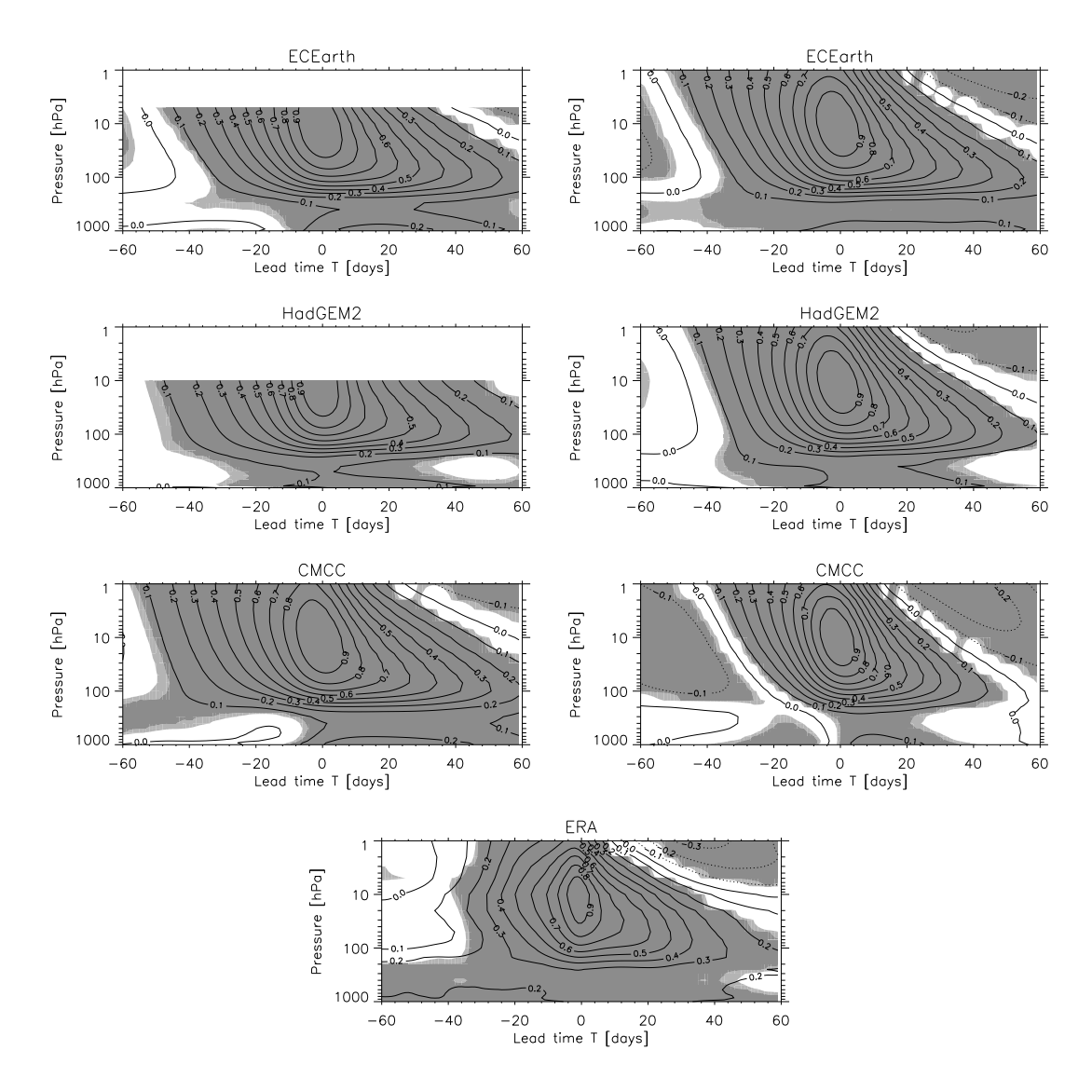


**Figure 10:** The lagged correlations between the zonal mean zonal wind at 10 hPa, 60°N and zonal mean zonal winds at other levels. Left panels: low top experiments (EC-Earth and HadGEM; for CMCC on the left side the low-resolution high-top results are reported). Right panels: high top experiments. Shading indicates regions where the correlations are significantly different from zero at the 99% and 95% levels according to a Monte Carlo test. The period considered is 1900-2005 for the models and 1960-2005 for the ERA-40 reanalysis.

The changes in the time-scales are more clearly seen in Figure 11 where the auto-correlations of the zonal mean zonal winds are shown for 10 hPa and at the near-surface level. At 10 hPa both versions of EC-Earth and HadGEM overestimate the correlations between 25 and 65 days with the largest overestimation for the low top version of HadGEM. For the CMCC model the low resolution version is found to seriously overestimate the correlations for all lags whereas the high resolution version seriously underestimates all correlations. At the surface both versions of EC-Earth and HadGEM catch the observed correlations well. The low resolution version of CMCC

overestimates the correlations for lags out to 25 days but this has been corrected in the high resolution version (consistent with Gerber et al., 2008).

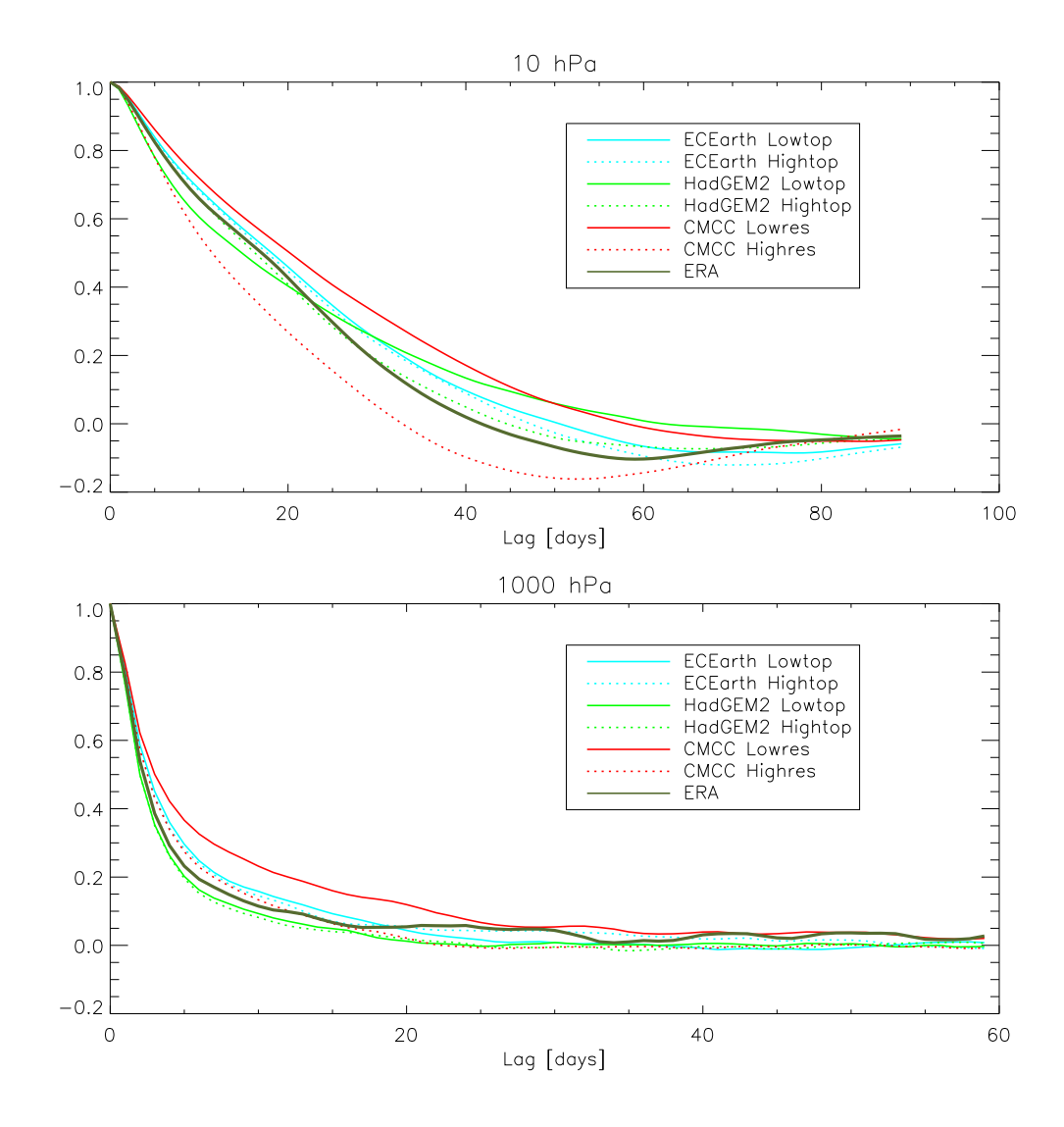


**Figure 11:** Autocorrelations of the zonal mean wind at 60°N as function of lag. Upper panel: 10 hPa. Lower panel: 1000 hPa.

The mean and temporal variability of the zonal mean zonal wind are now investigated. These quantities are tightly connected to the downward propagation; the downward propagation accounts for the majority of the variability in extra-tropical winter and the mean state guides the propagation of planetary waves which drive the downward propagation.

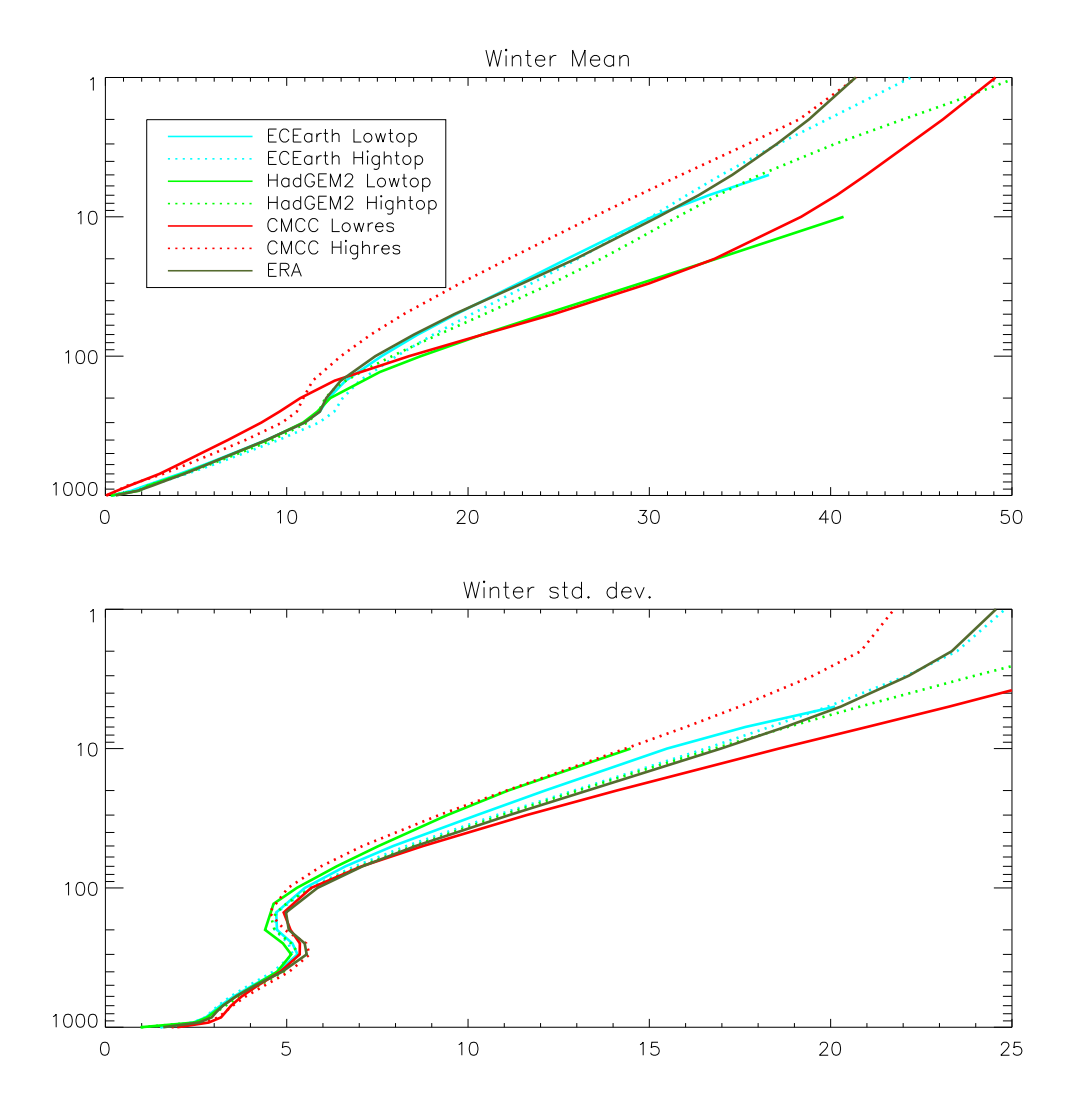


**Figure 12:** Mean (top) and standard deviation (bottom) [m/s] of the zonal mean wind at 60°N as a function of altitude. The annual cycle is removed before the calculation of the standard deviation.

The winter mean and standard deviation of the zonal mean zonal wind at 60°N are shown in Figure 12 as a function of altitude for the different model versions and for the ERA-40 reanalysis. Both versions of the EC-Earth model catch both mean and variability very well. The low top version of HadGEM overestimates the mean while this overestimation has been drastically improved in the high top version. The low resolution version of CMCC overestimates both the mean and the variability while high resolution version of CMCC underestimates both.

## 3.4.2 Stratospheric variability

The discussion above combines all thee winter months. Figure 13 shows the annual development of the zonal mean zonal wind at 60°N, 10 hPa. As expected all models reproduce the distinct seasonal profile with very weak variability in the summer and high variability in the winter. In the panels in the right column (showing high top versions) the purple lines show for which calendar days the distributions for the low top and high top versions are different at the 95% significance level (a Kolmogorov-Smirnov test with the effective number of data points taken as the number of years

(106) has been used). In all three models there is a significant difference between the two versions for nearly all calendar days (compare with Figure 12). However, for EC-Earth and HadGEM these significant differences are due to differences in the mean annual cycle. The calendar days for which the distributions for the low top and high top versions differ after the seasonal cycle is removed are marked with red in the right column of Figure 13. Only for CMCC, which differs also in horizontal resolution, is there a statistically significant difference in the variability. This difference is limited to the late winter and spring. When comparing to the ERA-40 reanalysis the briefer period 1960—2005 is used. However, the low top version of HadGEM and low resolution version of CMCC are still found to differ significantly from the reanalysis mostly because of differences in the annual cycle. These differences are less significant in the high top versions (not shown). Both versions of EC-Earth are comparable to the high top version of HadGEM and high resolution CMCC.

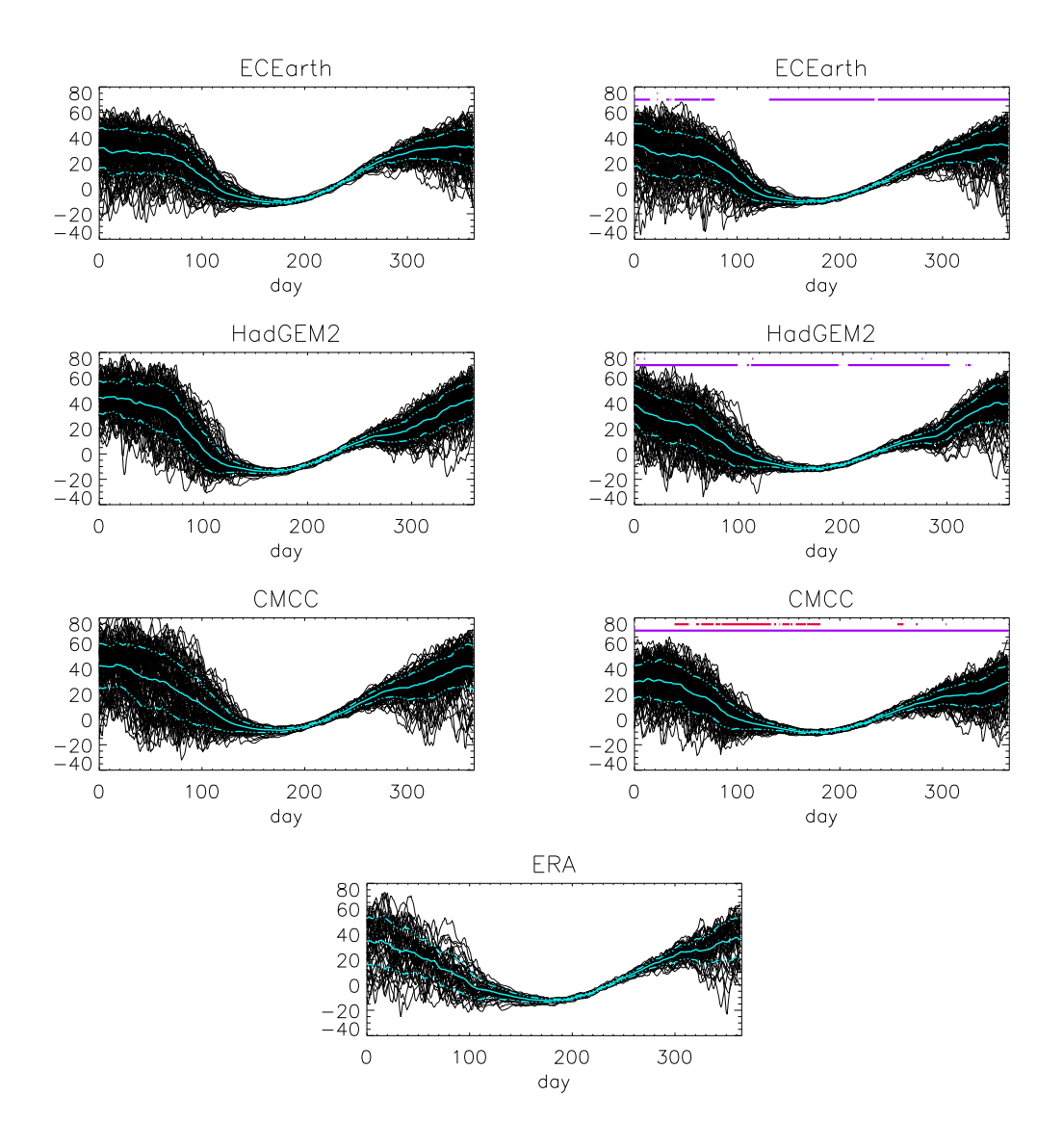


**Figure 13:** The seasonal cycle of the daily zonal mean wind [m/s] at  $60^{\circ}$ N at 10 hPa. Left panels: low top experiments (or low resolution CMCC-CESM). Right panels: high top experiments (or high resolution CMCC-CMS). Bottom: ERA-40. The period is 1900-2005 for the models and 1960-2005 for the reanalysis. Blue full curve is the mean seasonal cycle and dashed blue curves give  $\pm$  one standard deviation.

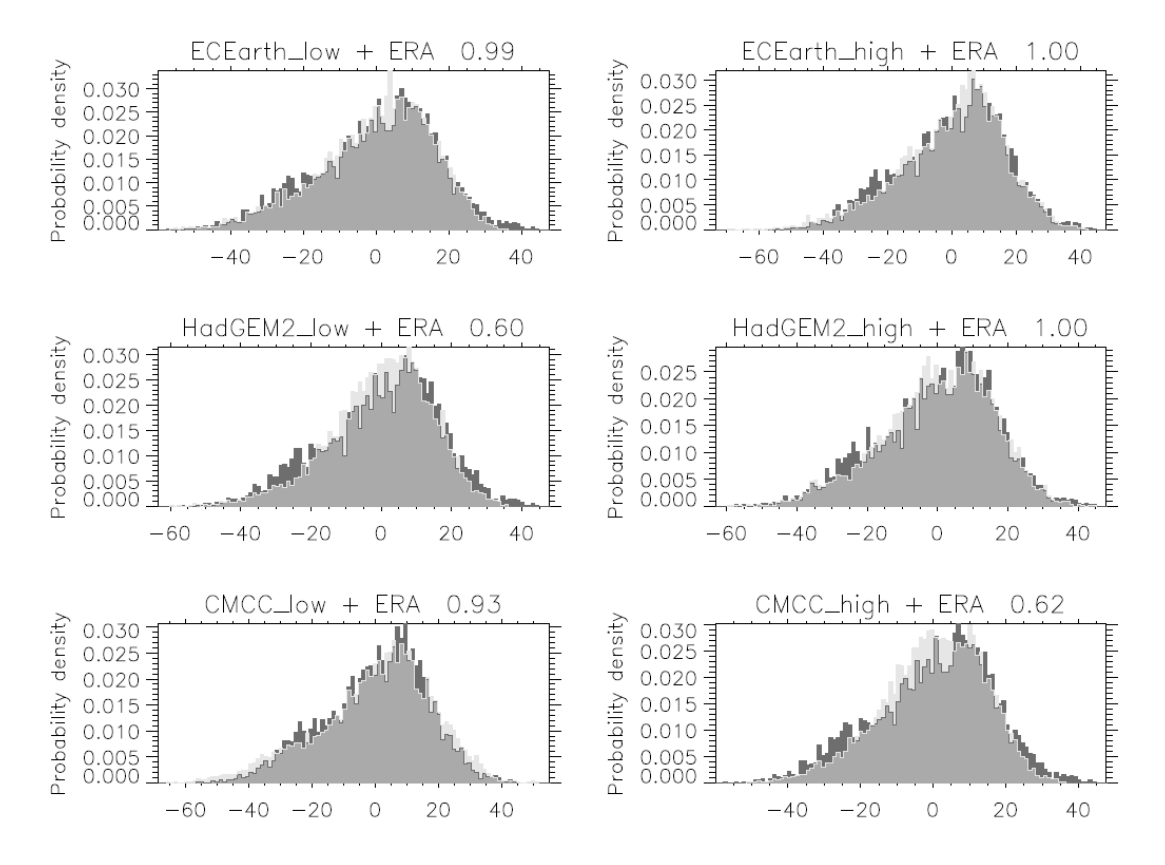


**Figure 14:** Histograms of winter daily zonal mean zonal wind [m/s] at 60°N, 10 hPa. Left panels: low top experiments (or low resolution CMCC-CESM). Right panels: high top experiments (or high resolution CMCC-CMS). Dark shading is ERA-40, light shading is models. The annual cycle has been removed. The period is 1900–2005 for the models and 1960–2005 for the reanalysis.

The variability in the winter stratosphere is remarkable as it is strongly non-Gaussian. This is a consequence of the competition between the relaxation towards a radiative equilibrium profile with strong westerly zonal mean zonal winds and wave driven excursions away from this profile. This makes the distribution of the stratospheric zonal mean zonal wind skewed towards easterly (negative) winds. The winter stratosphere is one of the few places where non-Gaussianity has been shown to be statistically significant in observations (see Christiansen, 2009, and references therein). Figure 14 shows the distributions of the daily zonal mean zonal wind at 60°N, 10 hPa for the three winter months after the seasonal cycle has been removed. These distributions are shown together with the equivalent distribution from the reanalysis. The skewness in the ERA-40 data is -0.39 and the values for the EC-Earth and HadGEM low top models and CMCC low resolution model are -0.59, -0.52, and -0.51 respectively, and for the high top/high resolution versions are -0.59, -0.43, and -0.42. Thus, all model versions show negative skewness comparable to the reanalysis although it is somewhat too strong. For the HadGEM and CMCC models some improvement is found in the high top/fine resolution versions when compared to the low top/coarse resolution versions.

#### 4. Conclusions

Aspects of stratosphere—troposphere dynamical feedback have been considered using a set of five Earth System Models that contain a well resolved stratosphere. The influence of the stratosphere on tropospheric climate was investigated by comparing the results from these high top models to those from equivalent low top models. Several aspects of tropospheric dynamics and circulation are found to benefit from the inclusion of a well resolved stratosphere in Earth System Models.

The observed trends in the Southern Hemisphere (SH) tropospheric circulation patterns during SH summer are fully reproduced by the high top CMCC and IPSL models, whilst the low top CMCC models fail to reproduce both the amplitude and the timing of these patterns. As the imposed ozone changes are the same for high and low top model simulations, the differences can be ascribed to the poor representation of the stratospheric dynamics in the low top models.

The North Atlantic Oscillation (NAO) is well simulated by both high and low top models, all showing realistic interannual variability of the NAO index. The well known link between the NAO index and stratospheric jet strength is found here in all models. However, despite realistic interannual variability in stratospheric jet strength in all models, the interannual correlation between the NAO index and stratospheric jet strength is greater in high top models, suggesting that a well resolved stratosphere is required to fully capture the link between them. This implies that a well resolved stratosphere is required to accurately simulate the NAO index on year-to-year timescales. The high top model projection of MSLP onto the NAO index is in better agreement with ERA-40 than the low top model projection, suggesting that the teleconnections between the NAO index and the North Pacific, and also between the NAO index and Asia, are more accurately simulated in the high top models.

The model high top minus low top differences seen in the blocking index show that inclusion of a well resolved stratosphere improves the bias in this index, although in most locations the improvements are not large compared to the overall bias. The bias is reduced over the Atlantic and north Pacific regions by the inclusion of a well resolved stratosphere, but it is increased in other regions.

Comparing high and low top versions of EC-Earth and HadGEM, and high and low resolution versions of CMCC, it is found that while all the models show a downward propagation from the stratosphere to the troposphere there are differences in both stratospheric and tropospheric time-scales. In general the high top and high resolution versions compare more favourably with the reanalysis than do the low top and low resolution versions.

#### References

Ambaum, M. H. P. and B. R. Hoskins, 2002: The nao troposphere-stratosphere connection. *J. Climate*, **15**, 1969–1978.

Baldwin, M. P. and T. J. Dunkerton, 1999: Propagation of the arctic oscillation from the stratosphere to the troposphere. *J. Geophys. Res.*, **104**, 30 937–30 946.

Baldwin, M. P., D. B. Stephenson, D. W. J. Thompson, T. Dunkerton, A. J. Charlton, and A. O'Neill, 2003: Stratospheric memory and extended-range weather forecasts. *Science*, **301**, 636–640.

Baldwin, M. P. and D. W. J. Thompson, 2009: A critical comparison of stratosphere-troposphere coupling indices. *Q. J. R. Meteorol. Soc.*, **135**, 1661–1672.

Buehler, T., C. C. Raible, and T. F. Stocker, 2010: The relationship of winter season North Atlantic blocking frequencies to extreme cold or dry spells in the ERA-40. *Tellus*, **63A**, 212—222.

Charlton, A. J., A. O'Neill, D. B. Stephenson, W. A. Lahoz, and M. P. Baldwin, 2003: Can knowledge of the state of the stratosphere be used to improve statistical forecasts of the troposphere? *Q. J. Roy. Met. Soc.*, **129**, 3205–3224.

Christiansen, B., 1999: Stratospheric vacillations in a general circulation model. *J. Atmos. Sci.*, **56**, 1858–1872.

Christiansen, B., 2001: Downward propagation of zonal mean zonal wind anomalies from the stratosphere to the troposphere: Model and reanalysis. *J. Geophys. Res.*, **106**, 27 307–27 322.

Christiansen, B., 2005: Downward propagation and statistical forecast of the near surface weather. *J. Geophys. Res.*, **110**, D14 104, doi:10.1029/2004JD005431.

Christiansen, B., 2009: Is the atmosphere interesting? a projection pursuit study of the circulation in the northern hemisphere winter. *J. Climate*, **22**, 1239–1254.

D'Andrea, F., S. Tibaldi, M. Blackburn, G. Boer, M. Déqué, M. R. Dix, B. Dugas, L. Ferranti, T. Iwasaki, A. Kitoh, V. Pope, D. Randall, E. Roeckner, D. Straus, W. Stern, H. Van den Dool, and D. Williamson, 1998: Northern Hemisphere atmospheric blocking as simulated by 15 atmospheric general circulation models in the period 1979-1988. *Clim. Dyn.*, **14**, 385—407.

Dong, Buwen, Rowan T. Sutton, and Tim Woollings, 2010: Changes of interannual NAO variability in response to greenhouse gases forcing. *Clim. Dyn.*, **37(7-8)**, 1621–1641, doi:10.1007/s00382-010-0936-6

Folland, Chris K., Jeff Knight, Hans W. Linderholm, David Fereday, Sarah Ineson, and James W. Hurrell, 2009: The Summer North Atlantic Oscillation: Past, Present, and Future. J. Climate, 22, 1082–1103.

Gerber, E. P., S. Voronin, and L. M. Polvani, 2008: Testing the Annular Mode Autocorrelation Timescale in Simple Atmospheric General Circulation Models, MWR, 136, 1523-1536

Gerber, E. P., et al., 2010: Stratosphere-troposphere coupling and annular mode variability in chemistry-climate models. *J. Geophys. Res.*, **115**, D00M06, doi:10.1029/2009JD013770.

Gong, D., and S. Wang, 1999: Definition of Antarctic Oscillation index. *Geophys. Res. Lett.*, **26(4)**, 459–462, doi:10.1029/1999GL900003.

Hazeleger, W., et al., 2011: Ec-earth v2.2: description and validation of a new seamless earth system prediction model. *Clim. Dyn.*, 1–19.

Osborn, T. J., and P. D. Jones, 2000: Air flow influences on local climate: observed United Kingdom climate variations. *Atmospheric Science Letters*, **1**, 62–74, doi:10.1006/asle.2000.0013

Perlwitz, J. and N. Harnik, 2004: Downward coupling between the stratosphere and troposphere: The relative roles of wave and zonal mean processes. *J. Climate*, **17**, 4902–4909.

Scaife, A. A., J. R. Knight, G. K. Vallis, and C. K. Folland, 2005: A stratospheric influence on the winter NAO and North Atlantic surface climate. *Geophys. Res. Lett.*, **32** (L18715), doi:10.1029/2005GL023226

Scaife, A., T. Woollings, J. Knight, G. Martin, and T. Hinton, 2010: Atmospheric blocking and mean biases in climate models. *J. Climate*, **23**, 6143—6152.

Scherrer, S., M. Croci-Maspoli, C. Schwierz, and C. Appenzeller, 2006: Two-dimensional indices of atmospheric blocking and their statistical relationship with winter climate patterns in the Euro-Atlantic region. *Int. J. Climatol.*, **26**, 233—249.

Siegmund, P., 2005: Stratospheric polar cap-mean height and temperature as extended-range weather predictors. *Mon. Weather. Rev.*, **133**, 2436–2448.

Sillmann, J., M. Croci-Maspoli, M. Kallache, and R. W. Katz, 2011: Extreme cold winter temperatures in Europe under the influence of North Atlantic atmospheric blocking. *J. Climate*, **24**, 5899—5913.

Son, S.-W., E. P. Gerber, J. Perlwitz, L. M. Polvani, N. P. Gillett, K.-H. Seo, V. Eyring, T. G. Shepherd, D. Waugh, H. Akiyoshi, J. Austin, A. Baumgaertner, S. Bekki, P. Braesicke, C. Bruhl, N. Butchart, M. P. Chipperfield, D. Cugnet, M. Dameris, S. Dhomse, S. Frith, H. Garny, R. Garcia, S. C. Hardiman, P. Jockel, J. F. Lamarque, E. Mancini, M. Marchand, M. Michou, T. Nakamura, O. Morgenstern, G. Pitari, D. A. Plummer, J. Pyle, E. Rozanov, J. F. Scinocca, K. Shibata, D. Smale, H. Teyssedre, W. Tian, and Y. Yamashita, 2010: Impact of stratospheric ozone on Southern Hemisphere circulation change: A multimodel assessment, *J. Geophys. Res.*, 115, D00M07, doi:10.1029/2010JD014271.

Song, Y. and W. A. Robinson, 2004: Dynamical mechanisms for stratospheric influences on the troposphere. *J. Atmos. Sci.*, **61**, 1711–1725.

Thorncroft, C. D., B. J. Hoskins, and M. E. McIntyre, 1993: Two paradigms of baroclinic-wave lifecycle behaviour. *Quart. J. Roy. Meteor. Soc.*, **119**, 17—55.

Tibaldi, S., and F. Molteni, 1990: On the operational predictability of blocking. *Tellus*, **42A**, 343—365.

Uppala, S. M., P. W. Kallberg, A. J. Simmons, U. Andrae, V. da Costa Bechtold, M. Fiorino, J. K. Gibson, J. Haseler, A. Hernandez, G. A. Kelly, X. Li, K. Onogi, S. Saarinen, N. Sokka, R. P. Allan, E. Andersson, K. Arpe, M. A. Balmaseda, A. C. M. Beljaars, L. van de Berg, J. Bidlot, N. Bormann, S. Caires, F. Chevallier, A. Dethof, M. Dragosavac, M. Fisher, M. Fuentes, S. Hagemann, E. H\_olm, B. J. Hoskins, L. Isaksen, P. A. E. M. Janssen, R. Jenne, A. P. McNally, J.-F. Mahfouf, J.-J. Morcrette, N. A. Rayner, R. W. Saunders, P. Simon, A. Sterl, K. E. Trenberth, A. Untch, D. Vasiljevic, P. Viterbo, and J. Woollen, 2005: The ERA-40 re-analysis. *Quart. J. Roy. Meteor. Soc.*, **131**, 2961—3012, doi: 10.1256/qj.04.176

Wallace, J. M., 2000: North Atlantic Oscillation/annular mode: Two paradigms – one phenomenon. *Quart. J. Roy. Meteor. Soc.*, **126** (**564**), 791–805.

Woollings, T., 2010: Dynamical influences on European climate: an uncertain future. *Phil. Trans. R. Soc. A*, **368**, 3733—3756.

Woollings, T., and M. Blackburn, 2012: The North Atlantic jet stream under climate change and its relation to the NAO and EA patterns. *J. Climate*, **25**, 886—902, 2012.